

# UC Davis

## UC Davis Previously Published Works

### Title

Changes in volumetric and metabolic parameters relate to differences in exposure to sub-concussive head impacts

### Permalink

<https://escholarship.org/uc/item/5812w8mh>

### Journal

Cerebrovascular and Brain Metabolism Reviews, 40(7)

### ISSN

1040-8827

### Authors

Champagne, Allen A

Coverdale, Nicole S

Germuska, Mike

et al.

### Publication Date

2020-07-01

### DOI

10.1177/0271678x19862861

### Copyright Information

This work is made available under the terms of a Creative Commons Attribution License, available at <https://creativecommons.org/licenses/by/4.0/>

Peer reviewed



# Changes in volumetric and metabolic parameters relate to differences in exposure to sub-concussive head impacts

Allen A Champagne<sup>1</sup> , Nicole S Coverdale<sup>1</sup>,  
Mike Germuska<sup>2</sup> , Alex A Bhogal<sup>3</sup> and Douglas J Cook<sup>1,4</sup>

## Abstract

Structural and calibrated magnetic resonance imaging data were acquired on 44 collegiate football players prior to the season (*PRE*), following the first four weeks in-season (*PTC*) and one month after the last game (*POST*). Exposure data collected from *g*-Force accelerometers mounted to the helmet of each player were used to split participants into HIGH ( $N = 22$ ) and LOW ( $N = 22$ ) exposure groups, based on the frequency of impacts sustained by each athlete. Significant decreases in grey-matter volume specific to the HIGH group were documented at *POST* ( $P = 0.009$ ), compared to baseline. Changes in resting cerebral blood flow ( $CBF_0$ ), corrected for partial volume effects, were observed within the HIGH group, throughout the season ( $P < 0.0001$ ), suggesting that alterations in perfusion may follow exposure to sub-concussive collisions. Co-localized significant increases in cerebral metabolic rate of oxygen consumption ( $CMRO_2|_0$ ) mid-season were also documented in the HIGH group, with respect to both *PRE*- and *POST* values. No physiological changes were observed in the LOW group. Therefore, cerebral metabolic demand may be elevated in players with greater exposure to head impacts. These results provide novel insight into the effects of sub-concussive collisions on brain structure and cerebrovascular physiology and emphasize the importance of multi-modal imaging for a complete characterization of cerebral health.

## Keywords

Brain structure, cerebral blood flow, cerebral metabolism, dual-calibrated fMRI, sub-concussive impacts

Received 16 January 2019; Accepted 11 June 2019

## Introduction

Athletes who participate in collision sports are exposed to a large number of sub-concussive head impacts within a season and throughout their career.<sup>1,2</sup> A sub-concussive impact occurs from a direct or indirect impact to the head, where mechanical forces are transferred to the brain and may alter axonal integrity<sup>3,4</sup> or neural functioning,<sup>5,6</sup> without the presence of clinical or neurobehavioral symptoms. This, along with increasing awareness that head trauma may induce long-term changes in neuroimaging biomarkers,<sup>7,8</sup> has led to growing interest in integrating multi-modal imaging with helmet biometrics to understand the effects of repeated head impacts on brain health. More insight on the vulnerability of cerebral tissues to repetitive head trauma may provide better understanding of the relationship between microvascular injury and the

origins of early pathologies observed in a sample of retired professional athletes.<sup>9,10</sup>

Recently, season-long exposure to repeated sub-concussive impacts in collegiate football players has been associated with an increase in cerebral blood flow

<sup>1</sup>Centre for Neuroscience Studies, Queen's University, Kingston, ON, Canada

<sup>2</sup>Cardiff University Brain Research Imaging Center, Cardiff University, Cardiff, UK

<sup>3</sup>Department of Radiology, University Medical Center Utrecht, Utrecht, The Netherlands

<sup>4</sup>Department of Surgery, Queen's University, Kingston, ON, Canada

### Corresponding author:

Douglas J Cook, Department of Surgery, Queen's University, Room 232, 18 Stuart St., Kingston, ON K7L 3N6, Canada.  
Email: dj.cook@queensu.ca

(CBF).<sup>11</sup> More importantly, these changes were more prominent in athletes who sustained greater counts of higher threshold impacts (>80g), on a per practice basis, suggesting that both the frequency and magnitude of sub-concussive collisions may contribute to transient changes in baseline cerebral physiology. In line with research on repetitive head impacts,<sup>7,12,13</sup> pathophysiological changes in resting cerebral perfusion may indicate alterations in metabolic demand, in response to the cumulative microtrauma and shear stresses that are transferred to cerebral tissues, upon exposure to sub-concussive trauma.<sup>7</sup> These force loading mechanisms may induce structural brain damage and neuropathological sequelae that are triggered independently of concussive symptoms,<sup>7</sup> which in turn, may increase cerebral regulatory processes that maintain basal neuronal activity, and possibly, respond to cellular injury.<sup>14</sup> Structural changes in grey-matter integrity following sub-concussive collisions may also bias perfusion-based findings, given that CBF is quantified per 100 g of tissue,<sup>15</sup> emphasizing the need to correct for possible changes in partial tissue volumes when assessing the effects of head impacts on cerebral physiology to avoid misinterpretation of results.

Despite evidence of changes in CBF,<sup>11</sup> little is known about the effects of repeated sub-concussive impacts on resting oxygen extraction fraction (OEF<sub>0</sub>), defined as the percentage of oxygen removed at the capillary level from the blood to the tissues. OEF<sub>0</sub> fluctuations counteract changes in CBF<sub>0</sub>, by way of the inverse relationship between capillary transit time (based on CBF<sub>0</sub>) and oxygen extraction.<sup>16,17</sup> Together, CBF<sub>0</sub> and OEF<sub>0</sub> provide direct insight into the homeostatic processes needed to maintain cerebral metabolism,<sup>16,17</sup> which can be measured using the cerebral metabolic rate of oxygen consumption (CMRO<sub>2</sub>).<sup>18–20</sup> From these measurements, changes in energy utilization may provide information about the link between exposure to sub-concussive impacts and local alterations in oxidative metabolic processes. Historically, the preferred method to map resting CMRO<sub>2</sub> (CMRO<sub>2|0</sub>) has been with triple oxygen positron emission tomography (O<sub>15</sub>-PET).<sup>21</sup> However, this method is not suitable for longitudinal studies due to the associated exposure to ionizing radiation. A recently proposed, and non-invasive, alternative is the so-called dual-calibrated fMRI method, or QUO<sub>2</sub> magnetic resonance imaging (MRI),<sup>22</sup> which utilizes the simultaneous acquisition of arterial spin labeling (ASL) and blood oxygen level-dependent (BOLD) data. This method allows for quantitative hemodynamic mapping of important physiological parameters including OEF<sub>0</sub>, and CMRO<sub>2|0</sub>, to gain insight into the physiological mechanisms underscoring changes in blood flow.

In this study, collegiate football players were followed longitudinally using volumetric and calibrated MRI to evaluate the effects of repeated sub-concussive head trauma on brain structure and resting cerebrovascular physiology. Measurements were recorded pre-season, within season and after a post-season recovery period, along with helmet accelerometry data, in order to relate the documented findings to cumulative exposure. We hypothesized that increases in CBF<sub>0</sub> relative to baseline would be observed in players with greater exposure to sub-concussive head impacts, and that these would be concurrent with elevated measurements of CMRO<sub>2|0</sub>. We also hypothesized that these parameters would return towards baseline at the post-season time point, after one month of rest with no exposure to repetitive head trauma. Finally, we predicted that players with higher exposure would also show significant changes in grey-matter volume over time, as an index for changes in the structural integrity of the brain.

## Material and methods

### Participants

This study was approved by the Queen's University Health Sciences Research Ethics Board (Kingston, ON, Canada), and informed consent was obtained from each participant. The study number was SURG-399-17 (file number: 6021022). The study was conducted in accordance with the Declaration of Helsinki. A total of 44 Canadian male collegiate football student-athletes, varying in positions, were recruited to participate in this study. All subjects were scanned before the season ('PRE' group), within two months prior to participation in full contact practices (Figure 1). None of the athletes enrolled in this study were recovering or suffering from post-concussion symptoms at the time of the scan, or in the year prior.

Neuroimaging was repeated in-season following the 14-day training camp period and the first two regular season games (post-training camp; 'PTC' group), and post-season, one month following the last competitive game ('POST' group; Figure 1). Of the 44 players recruited from baseline testing, nine were removed from the PTC cohort prior to scanning (three concussions and six season-ending injuries), for a total of 35 follow-up subjects. Of these 35 athletes, two sustained a concussion during the second half of the season, and two suffered a season-ending injury. Thus, a total of 31 players (Figure 1) from the original cohort returned for the final time point (POST), approximately 30 days after their last participation in contact activities.

At each time point, subjects were also asked to complete the symptom evaluation section of the Sport Concussion Assessment Tool (3rd edition; SCAT-3),<sup>23</sup>

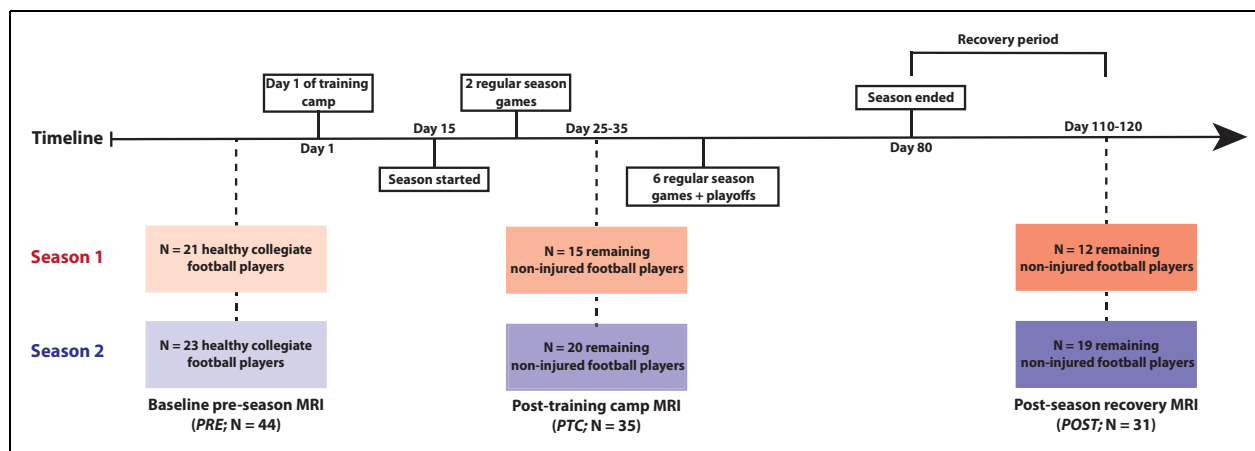


**Figure 1.** Schematic timeline of the study visits throughout the two seasons during which longitudinal data was collected. The timeline of the study design shows when subjects completed magnetic resonance imaging (MRI) with respect to the timing of the season; prior to training camp (PRE), following training camp and two season games (PTC), and one month following the last playoff game of the season (POST).

in order to monitor changes in self-rated symptoms throughout the season.

### Monitoring of head impact exposure per session

Cumulative exposure to sub-concussive head impacts was monitored for all participants using helmet-based accelerometers (gForce Tracker, GFT; Hardware version GFT3S ver4.0, Artaflex Inc., Markham, ON, Canada), which provided measures of linear acceleration ( $g$ ) and rotational velocity ( $^{\circ}/s$ ), by impact location. The head impacts were categorized as ‘top’, ‘front’, ‘right’, ‘left’, and ‘back’. Sensors were mounted inside the helmet shell, to the left of the crown air bladder.<sup>24</sup> Sensor data were collected during all games and practices (including training camp), using a trigger threshold of 15  $g$ , in order to comply with existing literature validating the GFT system.<sup>24</sup>

### Respiratory manipulations

Each session consisted of two functional MRI acquisitions collected separately with different breathing challenges: one hypercapnia (HC), and one hyperoxia (HO). The breathing manipulations consisted of a 2-min baseline period, followed by a block of gas inhalation (2-min for HC and 3-min for HO), and a 2-min recovery period (Figure 2(a)). A break of approximately 2 min was given to each subject between the protocols, during which additional imaging was acquired ( $M_0$ ; see below). HC and HO blocks were induced using a feed-forward computer-controlled gas blending system (RA-MR<sup>TM</sup>, Thornhill Research Inc., Toronto, ON), connected to a sequential gas delivery circuit. End-tidal pressures of carbon dioxide ( $P_{ET}CO_2$ )

and end-tidal pressure of oxygen ( $O_2$ ) ( $P_{ET}O_2$ ) were sampled continuously via lines connecting the subject to the automated system (Figure 2(a)). Prior to entering the magnet bore, subjects were fitted with a facemask sealed using adhesive tape (Tegaderm, 3M Health Care, St. Paul, MN, US). Subjects were then familiarized with the hypercapnic breathing paradigm using a condensed version of the protocol (1 min).

During HC,  $P_{ET}CO_2$  was targeted at 10 mmHg above the subject’s baseline using a hypercapnic gas mixture blended with medical (21:79% oxygen ( $O_2$ ): $N_2$ ) and carbon dioxide ( $CO_2$ ) enriched air (10:21:69%  $CO_2$ : $O_2$ : $N_2$ ).  $P_{ET}O_2$  was clamped at a baseline value of 110 mmHg. During HO,  $P_{ET}O_2$  was targeted at 300 mmHg, while  $P_{ET}CO_2$  was maintained at baseline values (Figure 2(a)).

### MRI data acquisition

Imaging data were acquired using a Siemens 3.0T Magnetom Tim Trio system with a 32-channel receiver head coil. A whole-brain  $T_1$ -weighted MP-RAGE (magnetization prepared rapid acquisition gradient echo) image was acquired for segmentation and registration using the following parameters: TR = 1760 ms, TE = 2.2 ms, time of inversion (TI) = 900 ms, voxel size = 1 mm isotropic, field of view (FOV) = 256 × 256 mm, flip angle = 9°, receiver bandwidth = 200 Hz/pixel, scan duration = 7 min and 32 s.

BOLD and CBF data were acquired simultaneously throughout the breathing manipulations using a dual-echo pseudo-continuous arterial spin labeling sequence (pCASL)<sup>25</sup> with echo planar imaging (EPI) readout: TR = 4000 ms, TE<sub>1</sub>/TE<sub>2</sub> = 10/30 ms, FOV = 250 × 250 mm, flip angle = 90°, voxel size = 3.9 mm isotropic, slice gap = 0.773 mm, label offset = 100 mm, receiver

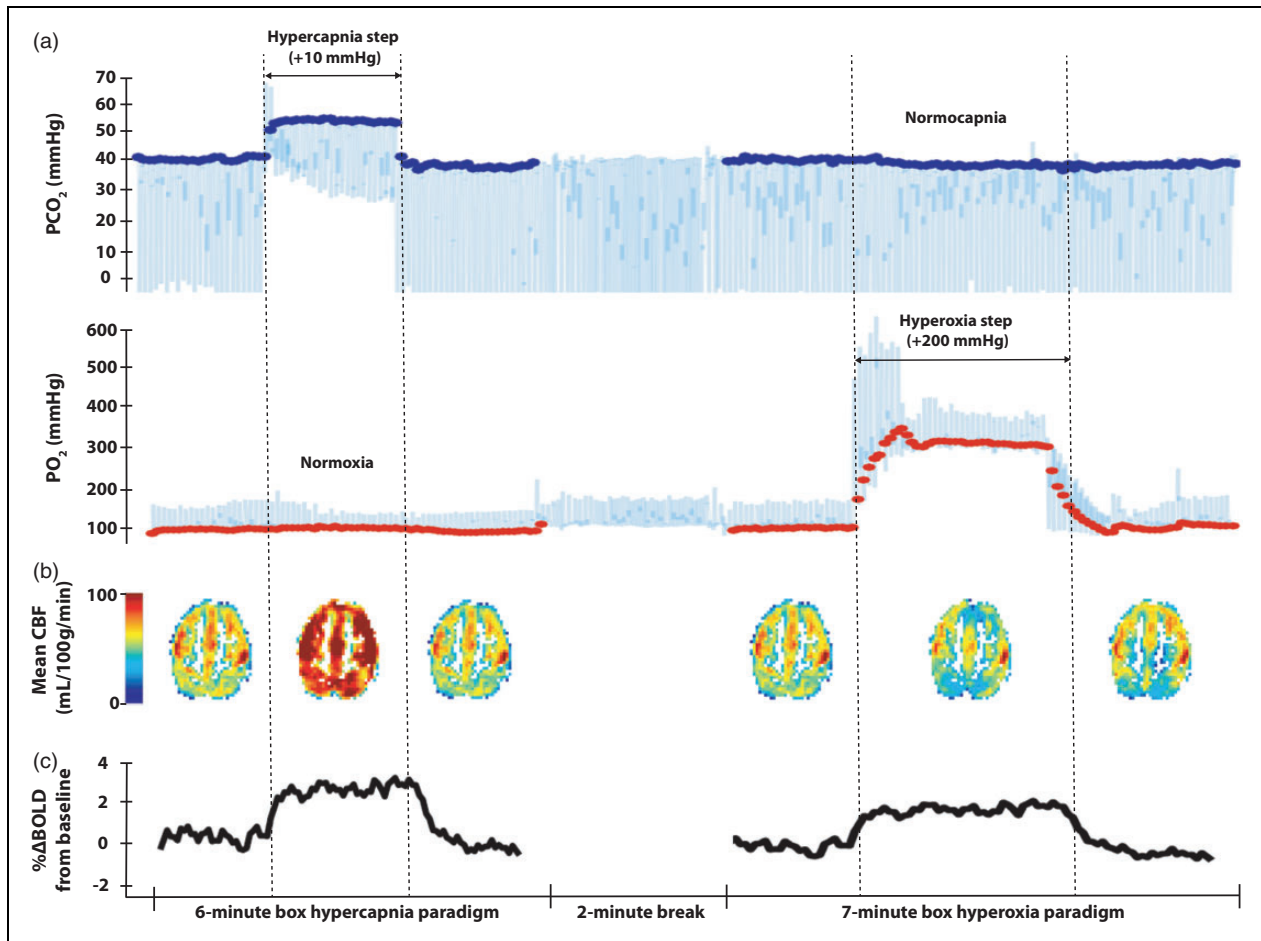


**Figure 2.** Example of the effects of the respiratory manipulations on perfusion and blood oxygen level-dependent signals in a representative participant. (a) The continuous trace (light blue) for  $P_{CO_2}$  (top) and  $P_{O_2}$  (bottom) sampled from the RA-MR™ (Thornhill Research Inc., Toronto, ON) are shown for both breathing manipulations. The end-tidal values for  $CO_2$  ( $P_{ET}CO_2$ ; navy filled circles) and  $O_2$  ( $P_{ET}O_2$ ; red filled circles) are also highlighted. The  $P_{ET}CO_2$  was targeted at 10 mmHg above the subject's baseline during hypercapnia. The  $P_{ET}O_2$  was targeted at 300 mmHg during hyperoxia. (b) Mean cerebral blood flow (CBF) maps for each period of the respiratory challenges (baseline, stimulus, recovery) shown in the subject's native space. (c) Mean grey-matter relative change in blood level oxygen dependent (BOLD) signal during each breathing manipulation over time.

bandwidth = 2604 Hz/pixel, and EPI factor = 64. The label duration was set to 1665 ms, while the post-labeling delay (PLD) ranged from 1000 to 2291 ms, based on the multislice single-shot EPI imaging readout, which caused a different PLD in each slice acquired (average PLD = 1646 ms). This correction was accounted for in the computation of CBF maps (see below). Twenty-five axial slices were acquired on a  $64 \times 64$  matrix (7/8 partial Fourier) in ascending order (i.e. bottom to top) for whole brain coverage using parallel imaging (GRAPPA acceleration factor = 2). For quantification of CBF, a tissue equilibrium magnetization map ( $M_0$ ) was acquired using the same pCASL parameters, with a longer TR (15,000 ms) and no spin labelling. EPI images were calibrated using a pre-scan normalized image acquired using the body transmit/receiver coil.

This step served to correct for inhomogeneities in the receive sensitivity of the 32-channel head coil.

### Data preprocessing

Data from this study were preprocessed using a combination of FSL,<sup>26</sup> AFNI,<sup>27</sup> and in-house designed Matlab (MATLAB 2018b, The MathWorks, Inc., Natick, Massachusetts, USA) scripts. Prior to reconstruction of each signal, non-brain tissues were removed using the brain extraction tool (BET), followed by automated motion correction (FSL *MCFLIRT*).<sup>28,29</sup> FSL's *epi\_reg* tool<sup>26</sup> was then used to co-register and align each subject's HO and HC in native space, while combining *topup*<sup>30,31</sup> and boundary-based registration<sup>32</sup> to improve alignment between

functional scans. Following automatic 3D segmentation of the structural  $T_1$  image (*FAST*),<sup>33</sup> the individual's extracted GM mask was re-sampled linearly into low-resolution native space using a reversed rigid-body transformation matrix (6 dof; *FLIRT*)<sup>28</sup> that aligned the EPI image to the structural anatomical scan.

BOLD images were isolated from the corrected pCASL series using a surround averaging of the second echo series ( $TE=30$  ms).<sup>34</sup> The BOLD data were then spatially smoothed using a Gaussian kernel of 8 mm with *SUSAN*,<sup>26</sup> and high-pass filtered<sup>26</sup> to address signal drift during the EPI acquisition. CBF data were reconstructed using a linear surround subtraction of the first-echo ASL image ( $TE=10$  ms), between the adjacent tag and control frames and spatially smoothed (8 mm full width at half maximum Gaussian kernel). To account for confounding effects of motion artefacts on ASL signal, and possible over-estimation of CBF, the BOLD and perfusion timeseries from each breathing paradigm were despiked (*3dDespike*, AFNI) using an upper range of 2.5 standard deviations. The perfusion data were then converted into absolute physiological units (mL/100 g tissue/min) using FSL's *oxford\_asl* toolbox,<sup>35</sup> with partial volume correction,<sup>36</sup> in order to reduce the partial volume effects from neighboring voxels containing a mixture of GM, white-matter and cerebrospinal fluid, as well as the possible confounding effects of changes in tissue integrity over time. The 't2star' option was also selected to correct for  $T_2^*$  effects in the computation of CBF maps. The differences in PLD between each slice (i) due to the two-dimensional EPI readout were accounted using  $PLD_i = 1000 \text{ ms} + (s_T) \times (i - 1)$ , where  $s_T$  represents the slice time in seconds ( $s_T = 53.8$  ms). For images acquired during baseline and HO breathing, the inversion efficiency ( $\alpha_{inv}$ ) was set to 0.84. During HC,  $\alpha_{inv}$  was set to 0.80 to account for the higher blood flow velocity in the feeding arteries, as a response to the higher arterial  $CO_2$  content.<sup>37</sup> The vasoconstrictive effects of HO on CBF<sup>38</sup> were obtained from the dual-echo imaging data and incorporated into the calibration model. To account for the reduction in arterial blood  $T_1$  ( $T_{1b}$ ) during HO, due to higher plasma concentration of paramagnetic  $O_2$ ,<sup>39,40</sup> the  $T_{1b}$  of blood was adjusted on a per-volume basis during CBF quantification based on the method proposed in Germuska et al. (Appendix A.1.2)<sup>41</sup> and the linear relationship between  $R_1$  and  $PaO_2$ .<sup>42</sup>

Grey-matter volume maps were computed using steps extracted from the voxel-based morphometry pipeline in FSL.<sup>31</sup> Briefly, segmented grey-matter tissues from the  $T_1$  anatomical scans were spatially transformed to the GM ICBM-152 template using affine (12 dof),<sup>28</sup> and non-linear warp-fields (*FNIRT*).<sup>43</sup> The spatially normalized maps were then used to create

a symmetric study-specific grey-matter template, in order to avoid biases in the analysis based on morphological differences in tissues across subjects. Individual grey-matter maps were finally re-registered non-linearly to the grey-matter template and multiplied by the Jacobian warp field ('modulation step'), followed by smoothing. These maps were then used for the volumetric statistical analysis of the grey-matter, over time (see below), based on exposure.

### Computation of hemodynamic parameter maps

The first 5 volumes of each pCASL timeseries were removed to allow the respiratory pattern to reach steady-state. Volumes acquired during baseline and stimulus periods were averaged (Figure 2) to create mean baseline, hypercapnic and hyperoxic images. Next, the BOLD and CBF signal changes associated with the step HC and HO (Figure 2(b) and (c)) were used to calculate the M parameter (the theoretical maximal percent change from complete removal of deoxy-hemoglobin), on a voxel by voxel basis, described in the original BOLD calibration model<sup>44</sup>

$$M = \frac{\frac{\Delta BOLD}{BOLD_0}}{1 - \left(\frac{CBF}{CBF_0}\right)^\alpha \cdot \left(\frac{[dHb]}{[dHb]_0}\right)^\beta} \quad (1)$$

In equation (1), and hereafter,  $BOLD_0$ , and  $CBF_0$  represent baseline values, whereas variables without subscripts represent fractional changes estimated from the HC and HO respiratory manipulation. These were calculated using the final 80 s period of the stimulus block (120 s), given that delays in the vascular response may affect the rapid transition period from baseline.<sup>45-47</sup> The Grubb coefficient ( $\alpha$ ), representing the non-linear coupling between flow and venous volume,<sup>48</sup> was set to 0.18.<sup>49</sup> The parameter  $\beta$ , which represents the non-linear relationship between changes in deoxy-hemoglobin concentration ( $[dHb]$ ) and  $R_2^*$ , was set to 1.3 (appropriate for field strength of 3.0 T).<sup>50</sup>

Baseline normalized  $[dHb]$  is a function of the changes in arterial oxygen content ( $C_aO_2$ ),  $OEF_0$ , and fluctuations in flow throughout the breathing protocols via equation (2)<sup>51</sup>

$$\frac{[dHb]}{[dHb]_0} = \left( \frac{\frac{Ca_{020} OEF_0}{x}}{1 - \frac{Ca_{020}}{x} (1 - OEF_0)} \right) \left( \frac{CBF_0}{CBF} \right) + \left( \frac{1 - \frac{Ca_{02}}{x}}{1 - \frac{Ca_{020}}{x} (1 - OEF_0)} \right) \quad (2)$$

where  $x = \varphi[Hb]$

In equation (2), the O<sub>2</sub> carrying capacity of hemoglobin ( $\varphi$ ) was set to 1.34 mL O<sub>2</sub>/g (Hb), while the total concentration of hemoglobin ([Hb]; oxygenated and deoxygenated) was assumed to be 15 g (Hb)/dL blood. Resting ( $C_aO_{210}$ ) and stimulus ( $C_aO_2$ ) oxygen content were derived using the Severinghaus equation<sup>52</sup> to get arterial hemoglobin saturation ( $S_aO_2$ ) and equation (3), which represents the sum of the oxygen bound to hemoglobin (first term) and dissolved in plasma (second term)

$$C_aO_2 = (\varphi \cdot [Hb] \cdot S_aO_2) + (P_aO_2 \times \varepsilon) \quad (3)$$

In equation (3),  $P_aO_2$  was replaced by the mean  $P_{ET}O_2$  for each block, and  $\varepsilon$  (0.0031 mL O<sub>2</sub>/dL blood/mm Hg), which represents the solubility of O<sub>2</sub> in plasma.<sup>51</sup>

M (equation (1)) and OEF<sub>0</sub> (equation (2)) were solved simultaneously on a voxel per voxel basis using the Gauthier method<sup>51</sup> to find a unique solution at the intersection of both functions, while integrating data from each breathing manipulation (see Figure 1 in Gauthier and Hoge<sup>51</sup> and Supplementary Figure 1(a) to (d)). Due to the low SNR in ASL, the low-resolution GM mask was used to limit the application of this method to GM voxels only, which are likely to provide better signal. Because flow changes in HO should be minimal,<sup>46,53,54</sup> the GM-averaged T<sub>1</sub>-corrected CBF for baseline and HO were used as inputs in equation (2) for the hyperoxic challenge. CMRO<sub>2</sub> was assumed to be constant ( $CMRO_2/CMRO_{210} = 1$ ) in this model (iso-metabolism).<sup>49</sup>

From here, individual voxelwise CMRO<sub>210</sub> maps corrected for partial volume effects were computed using

$$CMRO_{210} = CaO_{210} \cdot CBF_0 \cdot OEF_0 \cdot \left[ 39.34 \frac{\mu mol}{ml} \right] \quad (4)$$

where  $CBF_0$  was estimated from the baseline perfusion volumes preceding HC, with adjustments for partial volume estimates (Supplementary Figure 1(e) and (f)).

### Data analysis

Functional maps (e.g. CBF<sub>0</sub>, OEF<sub>0</sub>, and CMRO<sub>210</sub>) were warped into 2 mm Montréal Neurological Institute (MNI) space using concatenated linear and non-linear transformations that registered native images to standard space, via the high-resolution anatomical scan. Prior to alignment onto the standard template, the individuals' GM masks were filtered in low-resolution space using a T<sub>2</sub>\* map, which was derived from fitting the native multi-echo log-transformed signal with a linear regression ( $T_2^* = -\Delta TE / \log(\text{Signal}_{TE2} / \text{Signal}_{TE1})$ ; Supplementary Figure 2(a)).<sup>55</sup> This was done in order to eliminate voxels with baseline T<sub>2</sub>\* values below

30 ms, which are likely caused by susceptibility artefacts (Supplementary Figure 2(b)), and thus may bias the analysis of hemodynamic parameters over time. The subject's filtered GM mask (thresholded at 40%) was finally resampled into 2 mm MNI space, for further analysis of the physiological parameters.

Prior to the statistical analysis, two exposure groups were determined based on the daily exposure data recorded from the helmet accelerometers, between the *PRE* and *PTC* time points. Following computation of the average count of threshold impacts per session, the median of the sample was used to split the 44 participants into two equally sized groups: 'LOW' (below the median) and 'HIGH' (above the median) exposure. The LOW group served as the control for this analysis, in order to account for possible variations in CBF<sub>0</sub>, OEF<sub>0</sub>, and CMRO<sub>210</sub> over time that may be independent of exposure to sub-concussive impacts.

Volumetric and corrected CBF<sub>0</sub> maps were assessed for significant changes over time using a two by three factors mixed ANOVA, in order to account for each time point (within-subject; *PRE*, *PTC*, *POST*), both exposure groups (between-subject; LOW, HIGH), and missing data throughout the season due to injuries. This analysis was restricted to filtered GM voxels only. Significance from the voxelwise analysis was corrected for family-wise error at  $P < 0.05$  and a parameter-specific cluster size determined using Monte Carlo simulations (10,000 iterations) in AFNI's *3dFWHMx* (with spatial AutoCorrelation) and *3dClustSim*.<sup>56</sup> Significant clusters from the interaction between time and exposure were then used to extract regional volumetric and CBF<sub>0</sub> measurements and run post-hoc tests to understand the direction of the group differences based on time. Significant clusters from the CBF<sub>0</sub> analysis were also used to extract regional OEF<sub>0</sub> and corrected CMRO<sub>210</sub> values from each subject, in order to test for co-localized changes in metabolism, based on the effects of both exposure and time. Prior to the analysis of the regional values extracted from the clusters, the normality of each parameter's distribution was tested using the Shapiro-Wilk W-test. If not normally distributed, parameter values for each subject were log transformed before statistical comparison in IBM SPSS statistics (version 24.0, SPSS Inc., Chicago, IL, USA). Baseline P<sub>ET</sub>CO<sub>2</sub> values for each time point were used as a time-varying covariate variable when comparing CBF<sub>0</sub> and OEF<sub>0</sub>.

## Results

### Data-driven grouping for exposure based on helmet biometrics

The helmet accelerometer data were used to split subjects into a LOW and HIGH exposure group



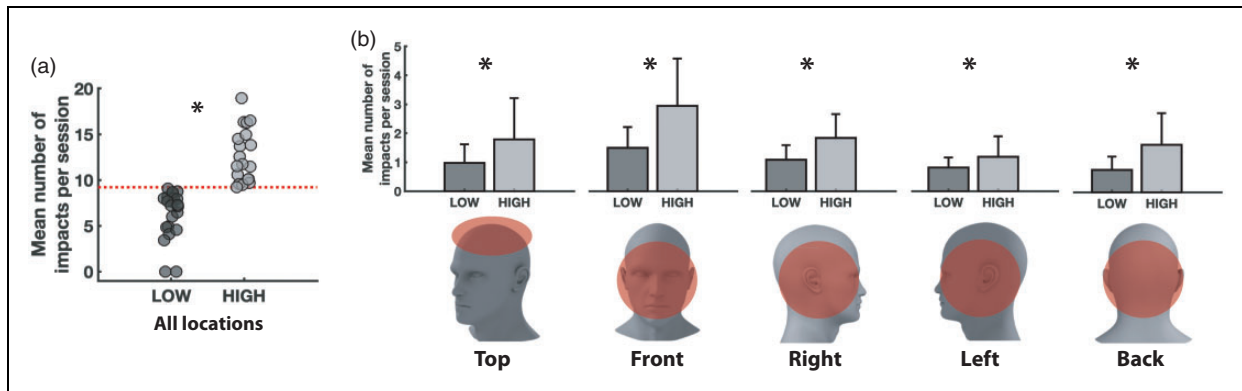


**Figure 3.** Data-informed grouping of the participants based on helmet accelerometer biometrics. (a) The LOW ( $N=22$ ) and HIGH ( $N=22$ ) groups were defined based on the average daily exposure to sub-concussive impacts (per session) having a linear acceleration of 15 g and above. Both practices and games were recorded for each participant and were used to characterize their exposure per session. The median (red dotted line; median = 9.21 head impacts per session) was used as the thresholding parameter. (b) The number of impacts per session for each location was compared between the groups showing that the HIGH exposure recorded higher counts of impacts on all sides of the helmet. \* $P < 0.05$  for a univariate ANOVA.

based on a median average frequency of impacts per session equal to 9.21 (Figure 3(a)). The LOW group (mean<sub>age</sub> = 20.2 ± 1.2 years, mean<sub>weight</sub> = 91.3 ± 13.2 kg, mean<sub>height</sub> = 184.8 ± 5.4 cm) consisted of eight defensive backs (DB), four defensive linemen (DL), one fullback (FB), one kicker (K), three linebackers (LB), one quarterback (QB), two safeties (S), and two wide-receivers (WR). The HIGH group (mean<sub>age</sub> = 19.7 ± 1.6 years, mean<sub>weight</sub> = 96.3 ± 11.8 kg, mean<sub>height</sub> = 185.8 ± 5.7 cm) included two DBs, five DLs, seven LBs, one offensive lineman (OL), one FB, one running back (RB), one S, two tight-ends (TE), and two WRs. The maximum number of impacts per session was also compared between the groups to show that HIGH exposure players sustained greater high impact sessions, relative to the LOW group (average maximum impacts in single session for LOW = 23.3 ± 10.4 impacts and HIGH = 42.6 ± 21.9 impacts;  $P < 0.0001$ ). There were no significant differences ( $P > 0.05$ ) in age, height or weight between the two exposure groups (i.e., LOW vs. HIGH).

Further statistical analysis of the helmet kinematic data based on the LOW vs. HIGH exposure groups showed that the HIGH exposure players also sustained greater average peak rotational velocity per session (LOW = 413.7 ± 54 °/s and HIGH = 456.5 ± 72 °/s;  $P = 0.018$ ), although no differences in mean linear acceleration per session were documented between the exposure groups (LOW = 31.1 ± 3.8 g and HIGH = 32.4 ± 3.5 g;  $P = 0.079$ ). Finally, statistical analyses of the count of impacts per location also revealed that the HIGH exposure group sustained more impacts on all sides of the helmet per session recorded, compared to the LOW exposure players (Figure 3(b)).

### Respiratory data

No significant differences in baseline  $P_{ET}CO_2$  and  $P_{ET}O_2$  were documented across the three time points, for each group, except small fluctuations (±3 mmHg) in  $P_{ET}O_2$  for the LOW exposure players (Table 1). Additionally, subjects from each group were exposed to similar hypercapnic and hyperoxic gas challenges during the breathing manipulations, indicated by the constant magnitude of change in  $P_{ET}CO_2$  and  $P_{ET}O_2$  across all time points (Table 1).

### Volumetric differences based on exposure and time

Overall, there were no significant interaction between exposure and time on the SCAT-3 symptom scale ( $P = 0.473$ ) and severity scores ( $P = 0.128$ ).

Voxelwise volumetric analysis of the grey-matter volume maps revealed a significant interaction between exposure and time over widespread regions of the brain (Figure 4). Five significant clusters (corrected for a minimum size of 148.6 voxels) were localized across both the left and right hemispheres, with specific focal points spread around the frontal, parietal, temporal, and occipital lobes (Table 2).

Post-hoc mixed ANOVA testing for the effect of time within each group indicated a difference in grey-matter volume for the HIGH exposure players over time ( $P = 0.026$ ). Further pairwise comparisons within this group showed that grey-matter volume was reduced ( $P = 0.009$ ) at *POST* ( $0.53 \pm 0.04 \text{ mm}^3$ ), in comparison to the *PRE*-season time point ( $0.55 \pm 0.03 \text{ mm}^3$ ). No significant differences were documented in the LOW group ( $P = 0.226$ ).



**Table 1.** End-tidal pressures of CO<sub>2</sub> and O<sub>2</sub> during baseline, hypercapnia, and hyperoxia in each exposure group.

	LOW				HIGH			
	PRE	PTC	POST	P	PRE	PTC	POST	P
<i>Hypercapnia</i>								
Baseline P <sub>ET</sub> CO <sub>2</sub> (mmHg)	40 (4)	40 (4)	39 (4)	0.051	41 (4)	40 (3)	40 (3)	0.936
Baseline P <sub>ET</sub> O <sub>2</sub> (mmHg)	110 (5)	111 (7)	108 (3)	0.101	108 (6)	106 (5)	107 (3)	0.556
ΔP <sub>ET</sub> CO <sub>2</sub> (mmHg)	9 (1)	9 (1)	9 (1)	0.871	8 (1)	8 (2)	9 (2)	0.169
ΔP <sub>ET</sub> O <sub>2</sub> (mmHg)	3 (3)	2 (6)	2 (2)	0.450	5 (3)	4 (4)	3 (3)	0.257
<i>Hyperoxia</i>								
Baseline P <sub>ET</sub> CO <sub>2</sub> (mmHg)	40 (5)	40 (4)	39 (5)	0.248	40 (4)	40 (3)	41 (4)	0.395
Baseline P <sub>ET</sub> O <sub>2</sub> (mmHg)	111 (6)	110 (3)	108 (3)	<b>0.041</b> <sup>^</sup>	108 (7)	105 (7)	108 (4)	0.065
ΔP <sub>ET</sub> CO <sub>2</sub> (mmHg)	-1 (1)	0 (1)	0 (1)	0.682	0 (1)	-1 (1)	0 (1)	0.717
ΔP <sub>ET</sub> O <sub>2</sub> (mmHg)	240 (40)	248 (39)	231 (43)	0.097	239 (46)	238 (39)	230 (42)	0.846

Note: Values are mean (standard deviation). Values for each group were statistically compared using a linear mixed model for repeated-measures. P<sub>ET</sub>CO<sub>2</sub>: end-tidal carbon dioxide; P<sub>ET</sub>O<sub>2</sub>: end-tidal oxygen; PRE: pre-season time point; PTC: post-training camp time point; POST: post-season time point. <sup>^</sup>P < 0.05 for POST vs. PRE time point.

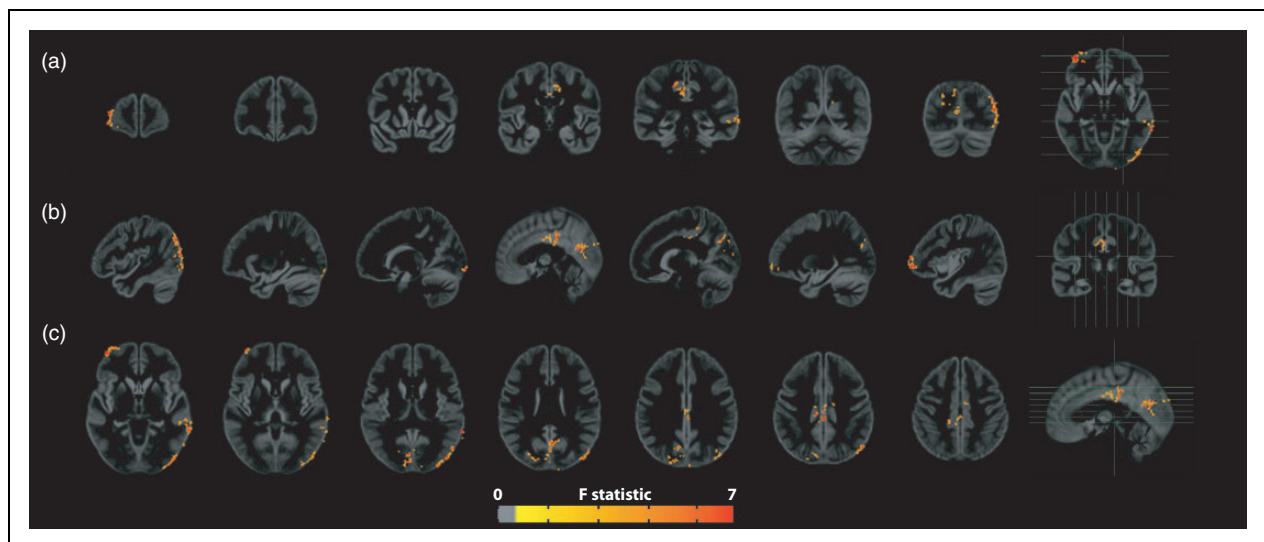


**Figure 4.** Significant clusters for the interaction between exposure and time on the volumetric data. Voxelwise two-by-three ANOVA corrected at  $P < 0.05$  for multiple comparisons (minimum cluster size 148.6 voxels) revealed widespread significant differences in grey-matter volume based on the interaction between exposure and time. Coronal (a), sagittal (b), and axial (c) slices of the statistical results are overlaid on the symmetric grey-matter template derived from the group data. The template was normalized to the 2 mm Montréal Neurological Institute (MNI) 2 mm atlas.

### Exposure-specific changes in hemodynamic parameters over time

T<sub>20</sub>\* filtering of the grey-matter maps removed approximately  $4 \pm 1\%$  of voxels, on average, across subjects. These were more often located within the temporal and inferior frontal lobes.

Voxelwise analysis of CBF<sub>0</sub> maps corrected for partial volume effects showed a significant interaction for time and exposure (Figure 5(a)) in three large clusters

(Table 2) spread over the frontal lobe and the superior region of the right and left parietal lobes. Post-hoc analysis of the regional perfusion measurements for the main effect of time showed that significant differences were driven by alterations in CBF<sub>0</sub> within the HIGH group (Figure 5(b);  $P = 0.001$ ). More specifically, CBF<sub>0</sub> was decreased at the POST time point, compared to both the PRE ( $P = 0.002$ ) and PTC ( $P < 0.0001$ ) measurements. CBF<sub>0</sub> at PTC was not statistically different compared to the PRE-season values ( $P = 0.203$ ) when

**Table 2.** Significant clusters from the voxelwise  $2 \times 3$  mixed ANOVAs on the volumetric and cerebral blood flow data showing a significant interaction between time and exposure.

Cluster	Size (voxels)	Center of mass (mm) <sup>a</sup>			Location
		X	Y	Z	
Volumetric data (grey-matter volume)					
1	546	-43	-82	12	Left middle occipital gyrus
2	372	6	-79	24	Right cuneus and right Brodmann area 18
3	276	2	-25	40	Right cingulate gyrus
4	187	-66	-42	2	Left middle temporal gyrus and left Brodmann area 22
5	178	36	60	-2	Right superior frontal gyrus and right Brodmann area 10
Cerebral blood flow (with partial volume correction)					
1	1417	-32	5	49	Left middle frontal gyrus and left Brodmann area 6
2	1069	26	-19	62	Right precentral gyrus and right Brodmann area 6
3	816	-34	-71	42	Left superior parietal lobule and left Brodmann areas 7 and 19

<sup>a</sup>Coordinates were converted from Talairach space to the Montreal Neurological Institute template and identified using the *3dclust* and *whereami* functions in AFNI. Clusters were thresholded at  $P < 0.05$  and a minimum size of 149 and 797.5 voxels for grey-matter volume and cerebral blood flow, respectively.

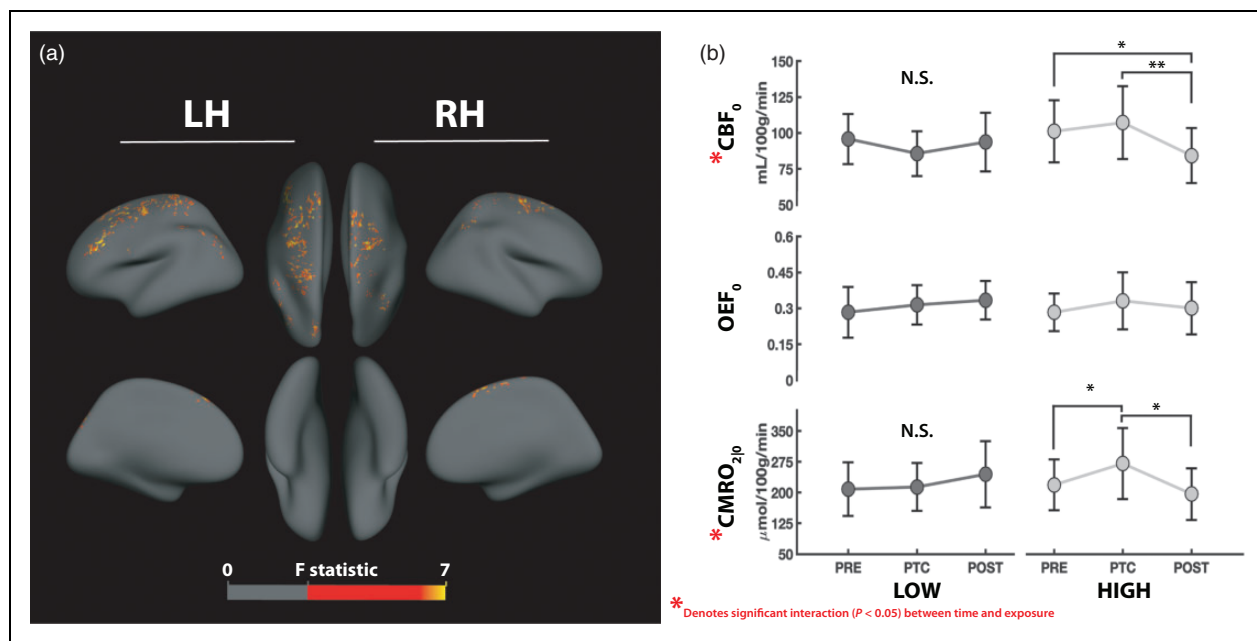


**Figure 5.** Significant results for the interaction between time and exposure in the voxelwise and region-of-interest analyses of the hemodynamic parameters. (a) Significant cluster from the voxelwise analysis of the baseline cerebral blood flow (CBF<sub>0</sub>) with partial volume correction adjusted for multiple comparisons at  $P < 0.05$  (minimum cluster size = 1324 voxels) showing the interaction between time and exposure. The statistical map is overlaid onto the freesurfer surface to show lateral, medial, superior and inferior views from the left (LH) and right (RH) hemispheres. (b) Post-hoc results showing mean ( $\pm$ standard deviation) regional CBF<sub>0</sub> (top), resting oxygen extraction fraction (OEF<sub>0</sub>), and cerebral metabolic rate of oxygen consumption (CMRO<sub>2j0</sub>) extracted for each exposure group (LOW = dark grey, HIGH = light grey) and time point (PRE, PTC, POST) within the significant cluster identified in (a). Time-varying end-tidal CO<sub>2</sub> was controlled for in the analysis of CBF<sub>0</sub> and OEF<sub>0</sub>. The red asterisk represents parameters (e.g. CBF<sub>0</sub> and CMRO<sub>2j0</sub>) that showed a significant interaction between time and exposure. \* $P < 0.05$ ; \*\* $P < 0.001$ ; N.S. = not significant.

corrected for the confounding effects of time-varying  $P_{ET}CO_2$  ( $P < 0.0001$ ).

In order to assess the physiological mechanisms underlying changes in perfusion, regional  $OEF_0$  and  $CMRO_{210}$  measurements were also extracted from the voxels highlighted in Figure 5(a). No significant interaction between exposure and time was observed for changes in  $OEF_0$ , and thus no further post-hoc tests were conducted. This was true for statistical testing of  $OEF_0$  with ( $P = 0.521$ ) and without ( $P = 0.596$ ) corrections for the confounding effect of  $P_{ET}CO_2$  over time ( $P < 0.0001$ ). Despite no change in  $OEF_0$ , significant fluctuations in regional  $CMRO_{210}$  were identified across time points, based on exposure (Figure 5(b);  $P = 0.029$ ). More specifically,  $CMRO_{210}$  measurements were found to change significantly over time for the HIGH group ( $P = 0.020$ ), with higher  $CMRO_{210}$  values observed at the *PTC* time point, compared to both the *PRE* ( $P = 0.035$ ) and *POST* ( $P = 0.008$ ) values. No significant differences were recorded between the *PRE* and *POST* time point ( $P = 0.345$ ). Lastly, no significant effect of time was documented within the LOW exposure group (Figure 5(b);  $P = 0.243$ ).

## Discussion

### Main findings

The present study is the first to combine volumetric and quantitative calibrated MRI, along with helmet accelerometers, to explore the effects of repeated sub-concussive impacts on brain structure and cerebral physiology. The main findings of this study are three-fold: (1) In the HIGH group, significant changes in grey-matter volume were observed following the season, after one month of no contact activity, suggesting that brain structure may be altered longitudinally following exposure to head impacts. (2) Decreased  $CBF_0$  after the season, corrected for partial volume differences, was specific to players with greater daily exposure to sub-concussive impacts. (3) Significant increases in  $CMRO_{210}$  mid-season were observed in the HIGH group, which, following one month post-season, returned to baseline values. Altogether, these findings support the hypothesis that exposure to repeated sub-concussive impacts to the head may be associated with sub-acute changes in brain structure and resting physiology, emphasizing the need to monitor the frequency of such impacts in football athletes throughout the season.

### Time-specific fluctuations in structural integrity and resting cerebrovascular physiology

Currently, the literature on the structural and neurophysiological effects of exposure to sub-concussive

impacts is limited.<sup>57</sup> However, some studies have demonstrated that subtle alterations in hippocampal volume,<sup>58</sup> cognitive function,<sup>5</sup> and biochemical and functional markers<sup>59-62</sup> can all be found in collision sport athletes, despite the lack of a diagnosed concussion. In this study, decreases in grey-matter volume were identified post-season in the HIGH group. This is in line with previous findings in soccer players,<sup>63,64</sup> suggesting that exposure to head impacts may be associated with structural differences longitudinally. Although some changes in hippocampal volume pre- and post-season were reported in Slobounov et al.,<sup>11</sup> these were not statistically significant, making findings from this study the first to be put forward in a cohort of collegiate football athletes and contribute to the literature on the effects of sub-concussive impacts on brain structure. Differences in grey-matter volume may indicate changes in the cellular integrity of the tissues,<sup>65</sup> although additional animal work is required to better understand the relationship between repeated micro-trauma and changes in tissue morphology.<sup>7</sup>

In addition to structural changes in the grey-matter, changes in perfusion were also specific to players within the HIGH group, suggesting that sub-concussive head impacts may be associated with transient changes in resting physiology. Here, lower resting perfusion was observed at the recovery time point (*POST*), relative to both *PRE* and *PTC* time points, suggesting that changes in regional brain perfusion persisted at one month following the end of the season, and no exposure to contact. No significant changes in  $CBF_0$  with respect to baseline were documented at the *PTC* time point, which differs from findings in Slobounov et al.,<sup>11</sup> who reported global and regional increases in resting perfusion following exposure to sub-concussive impacts. Differences in  $CBF_0$  reported in Slobounov et al.,<sup>11</sup> compared to this study, may be confounded by the differences in the length of exposure between the baseline and follow-up MRIs, which was much shorter in this study (~1 month), as opposed to an entire season in Slobounov et al.<sup>11</sup> Their design also did not account for time-varying changes in end-tidal  $CO_2$ , which was found to covary significantly with changes in  $CBF_0$ , in this study.

$CMRO_{210}$  was increased in the HIGH group after onset of participation in contact activities, which was in line with our original hypothesis. These results suggest that football players in the HIGH group had greater resting metabolic demand in-season, compared to both baseline and post-season time points. Group-specific differences in  $CMRO_{210}$  over time contribute evidence for the hypothesis that the frequency of sub-concussive impacts is related to changes in resting cerebral physiology, proposed by Slobounov et al.<sup>11</sup> Higher regional  $CMRO_{210}$  at the *PTC* time point may result

from regional increases in cellular  $O_2$  uptake due to inefficiencies in oxygen utilization,<sup>66</sup> or, greater consumption of energy (in the form of ATP) in order to meet elevated metabolic demands in response to shear stresses,<sup>14</sup> or trauma from mechanical stretch of the neurons.<sup>67</sup> In both scenarios, the observed increase in  $CMRO_{210}$  would ensure that the brain is supplied with adequate energy pre-cursors, which may be directed towards re-establishing ionic homeostasis and membrane potential disturbed following cellular damage.<sup>68–70</sup> While elevated  $CMRO_{210}$  measurements in the HIGH group returned towards baseline values one month following the end of the season,  $CBF_0$  was significantly reduced post-season within the region of interest (Figure 5(b)). In healthy tissues, decreases in  $CBF_0$  are typically counteracted with higher  $OEF_0$ , in order to maintain homeostatic balances between delivery, and consumption of oxygen. Here, in the HIGH group, persistent  $OEF_0$  values *POST*-season, in line with measurements from *PRE* and *PTC*, suggest that decreases in flow (or maintained  $OEF_0$  values) may be a physiological response from homeostatic mechanisms attempting to balance cerebral metabolic demands.

#### *Using helmet biometrics as an index for subject-specific differences in exposure to head impacts*

Knowledge about the differences in exposure to head impacts across football positions<sup>71,72</sup> has been used to classify players and explore the relationship between microtrauma and acute or long-term changes in brain biomarkers.<sup>6,73</sup> Although this is common practice, the distribution of positions between the LOW and HIGH group in this study suggests that careful consideration should be made when assigning athletes to different groups based on their predicted exposure to head impacts. It is likely that certain positions such as OLs, DLs, and LBs may often be assigned to the HIGH exposure group.<sup>72</sup> However, there also seems to be a certain degree of unpredictability and overlap in positions like WRs, DBs, and even DLs, who vary widely in terms of their exposure to head impacts per session, likely due to individual differences in playing style and technique. Additional factors like differences in aggressivity,<sup>74</sup> and/or starting status,<sup>1</sup> can also play a critical role in determining how often players sustain impacts to the head, during a certain time period. Thus, moving forward, neuroimaging studies of head impacts should strongly consider using helmet telemetry in order to properly identify hitting profiles within each athlete, and adequately separate participants based on their own individualized behavior, and not the expectation for a position, or body size.

#### *Limitations and future considerations*

During the calibration, [Hb] was assumed to remain constant across all time points throughout the season. However, possible variations in [Hb] over time, or between the groups, based on changes in hematocrit levels due to fitness<sup>75</sup> or mental stress<sup>76,77</sup> for instance, may also have contributed to the observed changes in resting cerebral metabolism. This effect was likely minimized in this design given that group-differences documented over time were extracted based on exposure to head impacts in players from varying positions, included in each experimental group (LOW vs. HIGH; see section 'Participants' section). Little to no differences in  $CMRO_{210}$  (or  $CBF_0$ ) were observed in players who sustained lower exposure to sub-concussive impacts during the timeline studied. Furthermore, because in-season training is heavily focused on strength and fitness maintenance built during the off-season, possible fluctuations in [Hb] over time may have been limited. Future designs should, however, aim to collect a sub-sample of blood in athletes studied, over time, in order to provide more insight about possible variations in [Hb] during the season and improve the calibration approach.

Other modeling parameters such as  $\alpha$  and  $\beta$  were chosen based on existing literature,<sup>51</sup> although more recent methods have presented novel ways to estimate such parameters.<sup>78</sup> These methods may improve the estimation of  $OEF_0$ , although they also present with methodological limitations and still require additional validation across different clinical populations. In this design, the  $\alpha$  constant was used to estimate changes in cerebral blood volume (CBV) indirectly via changes in  $CBF$  during the gas manipulations, based on the power-law relationship.<sup>48</sup> The lack of direct CBV measurements limits our ability to estimate regional  $CMRO_2$  using the biophysical model, as  $\alpha$  may vary depending on the experimental conditions.<sup>79</sup> Future designs may consider the use of vascular space occupancy (VASO)<sup>80</sup> in order to determine CBV experimentally,<sup>81</sup> and possibly improve calibrated  $CMRO_2$  measurements.<sup>82</sup>

In this study, a nominal PLD of 1000 ms was used to acquire the ASL signal, which was adjusted on a slice-by-slice basis due to the 2D EPI readout. ASL measurements of  $CBF$  are dependent on the selection of the PDL, which inherently relates to the longitudinal relaxation time of blood,<sup>83</sup> and the arterial transit time (ATT) from the labeling slice to the brain tissues.<sup>83,84</sup> ATT may vary across different regions of the brain, or between participants, which should be acknowledged when using ASL perfusion-based imaging in clinical population. No background suppression was employed in this imaging acquisition, although future design should also consider implementing such approach in order to improve SNR of the ASL signal.<sup>85</sup>

The effects of HC and HO on  $CMRO_2$  were assumed to be negligible in this study, although this remains a topic of debate.<sup>86–89</sup> Changes in  $CMRO_2$  during HC would violate an important assumption of the calibration model, which is that HC is assumed to be a purely vascular stimulus. Changes in  $CMRO_2$  would propagate into erroneous estimation of the M parameter, and thus,  $OEF_0$ . However, findings from the original calibration method suggests that potential changes in  $CMRO_2$  during HC are likely to be minimal.<sup>51</sup> This is further supported by the agreement between calibrated fMRI results from the studies reported above and the normative values published in the PET literature.<sup>90–92</sup>

In comparison to work using PET,<sup>93</sup> estimates of  $OEF_0$  and  $CMRO_{210}$  using calibrated fMRI have higher intra- and inter-subject variability,<sup>55,94</sup> likely due to the error propagation of the calibration. Reasons for this variability include the magnitude of the respiratory change in end-tidal measures,<sup>95</sup> along with variations across subjects, and between time points, in the vasoactive and vasoconstrictive effects of HC and HO on CBF, respectively. In earlier methods,<sup>44,51,54,96</sup> a  $T_1$ -corrected percent change in CBF was assumed based on the entire group's average decrease in flow, during HO. In this study, we estimated changes in arterial blood  $T_1$  during HO, and corrected CBF on an individual basis, which likely helped minimize potential intra-subject variation across time points. Fluctuations in  $P_{ET}CO_2$  between subjects and time points were also accounted for in our statistical model. Lastly, the effects of possible differences in  $OEF_0$  and  $CMRO_{210}$  within individuals, independent of exposure to head impacts, were also accounted for using the LOW group, which showed no significant variations over time, within the region of interest.

## Conclusion

In this study, volumetric and calibrated MRI were combined with helmet accelerometry to follow collegiate football athletes longitudinally and quantitatively record alterations in brain structure, and cerebral physiology, over time, and relate them to cumulative exposure to head impacts. Group-specific changes in grey-matter volume, resting perfusion, and metabolic demands were identified throughout the season for the HIGH exposure group only, suggesting that alterations in structure and physiology may be specific to players who sustain a greater frequency of impacts, on a daily basis. These findings provide novel insight about the effects of sub-concussive collisions, supporting the hypothesis that brain structural and hemodynamic parameters may vary in response to the mechanical loading sustained from head trauma. In the future, in-depth characterization of blood biomarkers and

neurocognitive function should also be included, in order to provide a comprehensive look at the relationship between neuroimaging findings, cognitive performance, biochemical changes, and repeated exposure to head impacts. Altogether, findings from this study contribute to advancing the literature on sub-concussive head impacts, while acting as a vehicle to make sport safer, and catalyzing the process by which we improve management of sub-concussive collisions in contact sports.

## Funding

The author(s) disclosed receipt of the following financial support for the research, authorship, and/or publication of this article: This work was funded by the Southeastern Ontario Academic Medical Organization (SEAMO).

## Acknowledgements

The authors of this paper would like to thank Mr. Don Brien and Mrs. Janet Mirtle-Stroman for their dedication and willingness to help with data collection. The authors would like to acknowledge Boris Baker and Emile Peponoulas for their help with collecting the helmet accelerometer data, along with the Queen's football program (Kingston, Ontario), for their generous contributions and participation in this research project. Finally, we would like to thank Dr. J. J. Wang at UCLA for sharing the pCASL sequence used in this study, Dr. Clarisse I. Mark for her insight regarding the method, and Artaflex Inc. for providing the gForce Tracker equipment.


## Declaration of conflicting interests


The author(s) declared no potential conflicts of interest with respect to the research, authorship, and/or publication of this article.

## Authors' contributions

AAC and NSC were responsible for the collection of the data. MG and AAB helped with the computational framework designed for the data analysis. AAC wrote the article and performed all analyses on the data. DJC supervised the project. All authors discussed the results and contributed to editing the final version of the article.

## ORCID iDs

Allen A Champagne  <https://orcid.org/0000-0003-0245-9627>

Mike Germuska  <https://orcid.org/0000-0003-0580-4350>

## Supplemental material

Supplemental material for this article is available online.

## References

1. Broglio SP, Eckner JT, Martini D, et al. Cumulative head impact burden in high school football. *J Neurotrauma* 2011; 28: 2069–2078.

2. Agel J and Harvey EJ. A 7-year review of men's and women's ice hockey injuries in the NCAA. *Can J Surg* 2010; 53: 319–323.
3. Bahrami N, Sharma D, Rosenthal S, et al. Subconcussive head impact exposure and white matter tract changes over a single season of youth football. *Radiology* 2016; 281: 919–926.
4. Davenport EM, Whitlow CT, Urban JE, et al. Abnormal white matter integrity related to head impact exposure in a season of high school varsity football. *J Neurotrauma* 2014; 8: 1–32.
5. Talavage TM, Nauman EA, Breedlove EL, et al. Functionally-detected cognitive impairment in high school football players without clinically-diagnosed concussion. *J Neurotrauma* 2014; 31: 327–338.
6. Clark MD, Varangis EML, Champagne AA, et al. Effects of career duration, concussion history, and playing position on white matter microstructure and functional neural recruitment in former college and professional football athletes. *Radiology* 2018; 286. DOI:10.1148/radiol.2017170539.
7. Tagge CA, Fisher AM, Minaeva OV, et al. Concussion, microvascular injury, and early tauopathy in young athletes after impact head injury and an impact concussion mouse model. *Brain* 2018; 141: 422–458.
8. Churchill NW, Hutchison MG, Di Battista AP, et al. Structural, functional, and metabolic brain markers differentiate collision versus contact and non-contact athletes. *Front Neurol* 2017. DOI:10.3389/fneur.2017.00390.
9. Baugh CM, Stamm JM, Riley DO, et al. Chronic traumatic encephalopathy: neurodegeneration following repetitive concussive and subconcussive brain trauma. *Brain Imaging Behav* 2012; 6: 244–254.
10. Omalu BI, DeKosky ST, Hamilton RL, et al. Chronic traumatic encephalopathy in a National Football League player. *Neurosurgery* 2006; 59: 1086–1092.
11. Slobounov SM, Walter A, Breiter HC, et al. The effect of repetitive subconcussive collisions on brain integrity in collegiate football players over a single football season: A multi-modal neuroimaging study. *NeuroImage Clin* 2017; 14: 708–718.
12. Sunami K, Nakamura T, Ozawa Y, et al. Hypermetabolic state following experimental head injury. *Neurosurg Rev* 1989; 12: 400–411.
13. Duckrow RB, Lamanna JC, Rosenthal M, et al. Oxidative metabolic activity of cerebral cortex after fluid-percussion head injury in the cat. *J Neurosurg* 1981; 54: 607–614.
14. Frangos JA, McIntire LV and Eskin SG. Shear stress induced stimulation of mammalian cell metabolism. *Biotechnol Bioeng* 1988; 32: 1053–60.
15. Zhao MY, Mezue M, Segerdahl AR, et al. A systematic study of the sensitivity of partial volume correction methods for the quantification of perfusion from pseudo-continuous arterial spin labeling MRI. *Neuroimage* 2017; 15: 384–397.
16. Coles JP, Fryer TD, Smielewski P, et al. Incidence and mechanisms of cerebral ischemia in early clinical head injury. *J Cereb Blood Flow Metab* 2004; 24: 202–211.
17. Vespa P, Bergsneider M, Hattori N, et al. Metabolic crisis without brain ischemia is common after traumatic brain injury: a combined microdialysis and positron emission tomography study. *J Cereb Blood Flow Metab* 2005; 25: 763–774.
18. Meyer J, Kondo A, Nomura F, et al. Cerebral hemodynamics and metabolism following experimental head injury. *J Neurosurg* 1970; 32: 304–319.
19. Nelson S, OHL and Passonneau JV. Changes in energy reserves in mouse brain associated with compressive head injury. In: Caveness WF and Walker AE (eds) *Head injury*. Philadelphia/Toronto: JB Lippincott, 1966, pp.444–447.
20. Nilsson B and Pontén U. Experimental head injury in the rat. Part 2: regional brain energy metabolism in concussive trauma. *J Neurosurg* 1977; 47: 252–61.
21. Anand SS, Singh H and Dash AK. Clinical applications of PET and PET-CT. *Med J Armed Forces India* 2009; 65: 353–8.
22. Hoge RD. Calibrated fMRI. *NeuroImage* 2012; 62: 930–937.
23. Concussion in Sport Group. *Sport concussion assessment tool*. 3rd Edition. *Br. J. Sports Med.* 2013; 47: 259.
24. Campbell KR, Warnica MJ, Levine IC, et al. Laboratory evaluation of the gForce Tracker™, a head impact kinematic measuring device for use in football helmets. *Ann Biomed Eng* 2016; 44: 1246–1256.
25. Alsop DC, Detre JA, Golay X, et al. Recommended implementation of arterial spin-labeled Perfusion mri for clinical applications: a consensus of the ISMRM Perfusion Study group and the European consortium for ASL in dementia. *Magn Reson Med* 2015; 73: 102–116.
26. Jenkinson M, Beckmann CF, Behrens TEJ, et al. Fsl. *Neuroimage* 2012; 62: 782–790.
27. Cox RW. AFNI: software for analysis and visualization of functional magnetic resonance neuroimages. *Comput Biomed Res* 1996; 29: 162–173.
28. Jenkinson M, Bannister P, Brady M, et al. Improved optimization for the robust and accurate linear registration and motion correction of brain images. *Neuroimage* 2002; 17: 825–841.
29. Jenkinson M and Bannister P. Improved methods for the registration and motion correction of brain images. *Neuroimage* 2002; 17: 825–841.
30. Andersson JLR, Skare S and Ashburner J. How to correct susceptibility distortions in spin-echo echo-planar images: application to diffusion tensor imaging. *Neuroimage* 2003; 20: 870–88.
31. Smith SM, Jenkinson M, Woolrich MW, et al. Advances in functional and structural MR image analysis and implementation as FSL Technical Report TR04SS2. *Neuroimage* 2004; 23(S1): 208–219.
32. Greve DN and Fischl B. Accurate and robust brain image alignment using boundary-based registration. *Neuroimage* 2009; 48: 63–72.
33. Zhang Y, Brady M and Smith S. Segmentation of brain MR images through a hidden Markov Random field model and the expectation-maximization algorithm. *IEEE Trans Med Imaging* 2001; 20: 45–57.



34. Smith SM and Brady JM. SUSAN – a new approach to low level image processing. *Int J Comput Vis* 1997; 23: 45–78.
35. Chappell MA, Groves AR, Whitcher B, et al. Variational Bayesian inference for a nonlinear forward model. *IEEE Trans Signal Process* 2009; 57: 223–236.
36. Chappell MA, Groves AR, MacIntosh BJ, et al. Partial volume correction of multiple inversion time arterial spin labeling MRI data. *Magn Reson Med* 2011; 65: 1173–83.
37. Aslan S, Xu F, Wang PL, et al. Estimation of labeling efficiency in pseudocontinuous arterial spin labeling. *Magn Reson Med* 2010; 63: 765–771.
38. Bulte DP, Chiarelli PA, Wise RG, et al. Cerebral perfusion response to hyperoxia. *J Cereb Blood Flow Metab* 2007; 27: 69–75.
39. Bhogal AA, Siero JC, Zwanenburg J, et al. Quantitative T1 mapping under precisely controlled graded hyperoxia at 7T. *J Cereb Blood Flow Metab* 2017; 37: 1461–1469.
40. Ma Y, Berman AJL and Pike GB. The effect of dissolved oxygen on the relaxation rates of blood plasma: implications for hyperoxia calibrated BOLD. *Magn Reson Med* 2016; 76: 1905–1911.
41. Germuska M, Merola A, Murphy K, et al. A forward modelling approach for the estimation of oxygen extraction fraction by calibrated fMRI. *Neuroimage* 2016; 139: 313–323.
42. Ma Y, Berman AJL and Pike GB. The effect of dissolved oxygen on relaxation rates of blood plasma. In: *Proceedings 22nd Scientific Meeting International Society for Magnetic Resonance in Medicine*. 2014, p. 3099.
43. Andersson JLR, Jenkinson M and Smith S. Non-linear registration aka Spatial normalisation FMRIB Technical Report TR07JA2. *In Pract* 2007; 22.
44. Davis TL, Kwong KK, Weisskoff RM, et al. Calibrated functional MRI: mapping the dynamics of oxidative metabolism. *Proc Natl Acad Sci U S A* 1998; 95: 1834–9.
45. Donahue MJ, Strother MK, Lindsey KP, et al. Time delay processing of hypercapnic fMRI allows quantitative parameterization of cerebrovascular reactivity and blood flow delays. *J Cereb Blood Flow Metab* 2016; 36: 1767–1779.
46. Champagne AA, Bhogal AA, Coverdale NS, et al. A novel perspective to calibrate temporal delays in cerebrovascular reactivity using hypercapnic and hyperoxic respiratory challenges. *Neuroimage* 2019; 187: 154–165.
47. Poub Blanc J, Crawley AP, Sobczyk O, et al. Measuring cerebrovascular reactivity: the dynamic response to a step hypercapnic stimulus. *J Cereb Blood Flow Metab* 2015; 35: 1746–1756.
48. Grubb RL, Raichle ME, Eichling JO, et al. The effects of changes in PaCO<sub>2</sub> on cerebral blood volume, blood flow, and vascular mean transit time. *Stroke* 1974; 5: 630–639.
49. Chen JJ and Pike GB. Global cerebral oxidative metabolism during hypercapnia and hypocapnia in humans: implications for BOLD fMRI. *J Cereb Blood Flow Metab* 2010; 30: 1094–1099.
50. Boxerman JL, Hamberg LM, Rosen BR, et al. Mr contrast due to intravascular magnetic susceptibility perturbations. *Magn Reson Med* 1995; 34: 555–566.
51. Gauthier CJ and Hoge RD. Magnetic resonance imaging of resting OEF and CMRO<sub>2</sub> using a generalized calibration model for hypercapnia and hyperoxia. *Neuroimage* 2012; 60: 1212–1225.
52. Severinghaus JW. Simple, accurate equations for human blood O<sub>2</sub> dissociation computations. *J Appl Physiol* 1979; 46: 599–602.
53. Gauthier CJ, Desjardins-Crépeau L, Madjar C, et al. Absolute quantification of resting oxygen metabolism and metabolic reactivity during functional activation using QUO<sub>2</sub> MRI. *Neuroimage* 2012; 63: 1353–1363.
54. Chiarelli PA, Bulte DP, Wise R, et al. A calibration method for quantitative BOLD fMRI based on hyperoxia. *Neuroimage* 2007; 37: 808–820.
55. Lajoie I, Tancredi FB and Hoge RD. Regional reproducibility of BOLD calibration parameter M, OEF and resting-state CMRO<sub>2</sub> measurements with QUO<sub>2</sub> MRI. *PLoS One* 2016; 11: 31.
56. Cox RW, Chen G, Glen DR, et al. FMRI Clustering in AFNI: false-positive rates redux. *Brain Connect* 2017; 7: 152–171.
57. Tarnutzer AA, Straumann D, Brugger P, et al. Persistent effects of playing football and associated (subconcussive) head trauma on brain structure and function: a systematic review of the literature. *Br J Sports Med* 2017; 51: 1592–1604.
58. Singh R, Meier TB, Kuplicki R, et al. Relationship of collegiate football experience and concussion with hippocampal volume and cognitive outcomes. *J Am Med Assoc* 2014; 311: 1883–1888.
59. Breedlove EL, Robinson M, Talavage TM, et al. Biomechanical correlates of symptomatic and asymptomatic neurophysiological impairment in high school football. *J Biomech* 2012; 45: 1265–1272.
60. Abbas K, Shenk TE, Poole VN, et al. Alteration of default mode network in high school football athletes due to repetitive subconcussive mild traumatic brain injury: a resting-state functional magnetic resonance imaging study. *Brain Connect* 2015; 5: 91–101.
61. Poole VN, Abbas K, Shenk TE, et al. MR spectroscopic evidence of brain injury in the non-diagnosed collision sport athlete. *Dev Neuropsychol* 2014; 39: 459–473.
62. Champagne AA, Coverdale NS, Nashed JY, et al. Resting CMRO<sub>2</sub> fluctuations show persistent network hyper-connectivity following exposure to sub-concussive collisions. *NeuroImage Clin* 2019; 22: 101753.
63. Koerte IK, Mayinger M, Muehlmann M, et al. Cortical thinning in former professional soccer players. *Brain Imaging Behav* 2016; 10: 792–798.
64. Adams J, Adler CM, Jarvis K, et al. Evidence of anterior temporal atrophy in college-level soccer players. *Clin J Sport Med*, Epub ahead of print 2007. DOI: 10.1097/JSM.0b013e31803202c8.
65. Morley WA. Environmental subconcussive injury, axonal injury, and chronic traumatic encephalopathy. *Frontiers in Neurology*, Epub ahead of print 2018. DOI: 10.3389/fneur.2018.00166.
66. Wagner BA, Venkataraman S and Buettner GR. *The rate of oxygen utilization by cells*. 2011; Epub ahead of print 2011. DOI: 10.1016/j.freeradbiomed.2011.05.024. The.



67. Geddes-Klein DM, Schiffman KB and Meaney DF. Mechanisms and consequences of neuronal stretch injury *in vitro* differ with the model of trauma. *J Neurotrauma* 2006; 23: 193–204.
68. Hovda DA, Fu K, Badie H, et al. Administration of an omega-conopeptide one hour following traumatic brain injury reduces 45 calcium accumulation. *Acta Neurochir Suppl* 1994; 60: 521–523.
69. Sutton RL, Hovda DA, Adelson PD, et al. Metabolic changes following cortical contusion: relationships to edema and morphological changes. *Acta Neurochir Suppl* 1994; 60: 446–448.
70. Yoshino A, Hovda D a, Kawamata T, et al. Dynamic changes in local cerebral glucose utilization following cerebral concussion in rats: evidence of a hyper- and subsequent hypometabolic state. *Brain Res* 1991; 561: 106–119.
71. Cantu RC. Frequency and location of head impact exposures in individual collegiate football players. *Yearb Sport Med* 2011; 2011: 20–22.
72. Crisco JJ, Fiore R, Beckwith JG, et al. Frequency and location of head impact exposures in individual collegiate football players. *J Athl Train* 2010; 45: 549–559.
73. Lehman EJ, Hein MJ, Baron SL, et al. Neurodegenerative causes of death among retired National Football League players. *Neurology* 2012; 79: 1970–4.
74. Schmidt JD, Pierce AF, Guskiewicz KM, et al. Safe-play knowledge, aggression, and head-impact biomechanics in adolescent ice hockey players. *J Athl Train*, Epub ahead of print 2016. DOI: 10.4085/1062-6050-51.5.04.
75. Mairbäurl H. Red blood cells in sports: effects of exercise and training on oxygen supply by red blood cells. *Front Physiol* 2013; 12: 332.
76. Patterson SM, Krantz DS, Gottdiener JS, et al. Prothrombotic effects of environmental stress: changes in platelet function, hematocrit, and total plasma protein. *Psychosom Med* 57: 592–599.
77. Ring C, Patterson SM, Bacon SL, et al. Reliability of hematocrit during rest and stress in healthy adults. *Biol Psychol* 2008; 77: 63–68.
78. Merola A, Murphy K, Stone AJ, et al. Measurement of oxygen extraction fraction (OEF): an optimized BOLD signal model for use with hypercapnic and hyperoxic calibration. *Neuroimage* 2016; 129: 159–174.
79. Kida I, Rothman DL and Hyder F. Dynamics of changes in blood flow, volume, and oxygenation: implications for dynamic functional magnetic resonance imaging calibration. *J Cereb Blood Flow Metab* 2007; 27: 690–696.
80. Lu H, Golay X, Pekar JJ, et al. Functional magnetic resonance imaging based on changes in vascular space occupancy. *Magn Reson Med* 2008; 60: 380–9.
81. Yang Y, Gu H and Stein EA. Simultaneous MRI acquisition of blood volume, blood flow, and blood oxygenation information during brain activation. *Magn Reson Med*, Epub ahead of print 2004. DOI: 10.1002/mrm.20302.
82. Lin AL, Fox PT, Yang Y, et al. Evaluation of MRI models in the measurement of CMRO<sub>2</sub> and its relationship with CBF. *Magn Reson Med*, Epub ahead of print 2008. DOI: 10.1002/mrm.21655.
83. Zhang X, Petersen ET, Ghariq E, et al. In vivo blood T1 measurements at 1.5 T, 3 T, and 7 T. *Magn Reson Med* 2013; 70: 1082–1086.
84. Lu H, Clingman C, Golay X, et al. Determining the longitudinal relaxation time (T1) of blood at 3.0 tesla. *Magn Reson Med* 2004; 52: 679–682.
85. Ye FQ, Frank JA, Weinberger DR, et al. Noise reduction in 3D perfusion imaging by attenuating the static signal in arterial spin tagging (ASSIST). *Magn Reson Med* 2000; 44: 92–100.
86. Horvath I, Sandor NT, Ruttner Z, et al. Role of nitric oxide in regulating cerebrocortical oxygen consumption and blood flow during hypercapnia. *J Cereb blood flow Metab* 1994; 14: 503–509.
87. Kety SS and Schmidt CF. The effects of altered arterial tensions of carbon dioxide and oxygen on cerebral blood flow and cerebral oxygen consumption of normal young men. *J Clin Invest* 1948; 27: 484–492.
88. Diringner MN, Aiyagari V, Zazulia AR, et al. Effect of hyperoxia on cerebral metabolic rate for oxygen measured using positron emission tomography in patients with acute severe head injury. *J Neurosurg* 2007; 106: 526–529.
89. Xu F, Uh J, Brier MR, et al. The influence of carbon dioxide on brain activity and metabolism in conscious humans. *J Cereb Blood Flow Metab* 2010; 31: 58–67.
90. Xu F, Ge Y and Lu H. Noninvasive quantification of whole-brain cerebral metabolic rate of oxygen (CMRO<sub>2</sub>) by MRI. *Magn Reson Med* 2009; 62: 141–148.
91. Ibaraki M, Shinohara Y, Nakamura K, et al. Interindividual variations of cerebral blood flow, oxygen delivery, and metabolism in relation to hemoglobin concentration measured by positron emission tomography in humans. *J Cereb Blood Flow Metab* 2010; 30: 1296–1305.
92. Ishii K, Sasaki M, Kitagaki H, et al. Regional difference in cerebral blood flow and oxidative metabolism in human cortex. *J Nucl Med* 1996; 37: 1086–1088.
93. Coles JP, Fryer TD, Bradley PG, et al. Intersubject variability and reproducibility of 15O PET studies. *J Cereb Blood Flow Metab* 2006; 26: 48–57.
94. Merola A, Germuska MA, Murphy K, et al. Assessing the repeatability of absolute CMRO<sub>2</sub>, OEF and haemodynamic measurements from calibrated fMRI. *Neuroimage* 2018; 173: 113–126.
95. Lajoie I, Tancredi FB and Hoge RD. The impact of inspired oxygen levels on calibrated fMRI measurements of M, OEF and resting CMRO<sub>2</sub> using combined hypercapnia and hyperoxia. *PLoS One* 2017; 12. DOI:10.1371/journal.pone.0174932.
96. Bulte DP, Kelly M, Germuska M, et al. Quantitative measurement of cerebral physiology using respiratory-calibrated MRI. *Neuroimage* 2012; 60: 582–591.